Journal Pre-proof

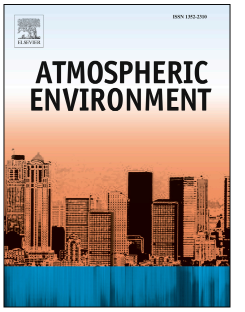

Aerosol data assimilation using data from Fengyun-4A, a next-generation geostationary meteorological satellite

Xiaoli Xia, Jinzhong Min, Feifei Shen, Yuanbing Wang, Dongmei Xu, Chun Yang, Peng Zhang

PII: S1352-2310(20)30427-1

DOI: https://doi.org/10.1016/j.atmosenv.2020.117695

Reference: AEA 117695

To appear in: *Atmospheric Environment*

Received Date: 9 January 2020

Revised Date: 3 June 2020

Accepted Date: 8 June 2020

Please cite this article as: Xia, X., Min, J., Shen, F., Wang, Y., Xu, D., Yang, C., Zhang, P., Aerosol data assimilation using data from Fengyun-4A, a next-generation geostationary meteorological satellite, *Atmospheric Environment* (2020), doi: https://doi.org/10.1016/j.atmosenv.2020.117695.

Author contributions:

Xiaoli Xia: Methodology, Software, Investigation, Run the experiments, Writing Original Draft.

Jinzhong Min: Collect data, choose the dust storm, Methodology, Validation, Supervision.

Feifei Shen: Data quality control, Validation, Formal analysis, Visualization.

Yuanbing Wang: Assimilation system construction, Edit code, Writing.

Dongmei Xu: Processing of observation data, Calculating the BEC, Writing.

Chun Yang: Writing – review & editing

Peng Zhang: Writing – review & editing

Aerosol data assimilation using data from Fengyun-4A, a next-generation geostationary meteorological satellite

Xiaoli XIA[1,*], Jinzhong MIN[1], Feifei Shen[1], Yuanbing Wang[1], Dongmei Xu[1], Chun Yang[1], Peng Zhang[2]

[1]*Key Laboratory of Meteorological Disaster of Ministry of Education (KLME)/Joint International Research Laboratory of Climate and Environment Change (ILCEC)/Collaborative Innovation Center on Forecast and Evaluation of Meteorological Disasters, Nanjing University of Information Science & Technology, Nanjing, China*

[2]*National Satellite Meteorological Center, China Meteorological Administration, Beijing, China*

* *Corresponding author:* Xiaoli Xia

xiaxl@nuist.edu.cn

Abstract

The Fengyun-4A (FY-4A) meteorological satellite, a next-generation geostationary meteorological satellite, was launched on 11 December 2016. For instance, the Advanced Geosynchronous Radiation Imager (AGRI) aboard FY-4A (AGRI/FY-4A) takes full-disk images at a 15-min interval in 14 spectral bands with the 0.5–4-km resolution. Here we developed data assimilation system based on the Gridpoint Statistical Interpolation (GSI) system in which the Aerosol Optical Depth (AOD) derived from FY-4A data were successfully assimilated for the first time. The capability to assimilate FY-4A Aerosol optical depth (AOD) with an hourly cycling configuration was then evaluated by a dust storm over East Asia during 12-14 May 2019. The analyses initialized Weather Research and Forecasting-Chemistry (WRF-Chem) model forecasts. The system is tested with FY-4 AOD, Himawari-8 AOD in experiments and then the results are compared to the Aerosol Robotic Network (AERONET) AOD observations, which serving as the independent observations. The results indicated that assimilating FY-4 AOD substantially showed much better agreement with observations than those from the control. Furthermore, the Bias and RMSE generally reduced about 20% with forecast range. This study indicates that the aerosol data assimilation using data from FY-4A can be used to improve the performance of forecast model.

Key words: Fengyun-4 satellite; aerosol optical depth; data assimilation; dust storm

1. Introduction

Economic growth has been very fast in China during the last decades (Chandran et al., 2013). The great increases in anthropogenic emissions during the last decades have caused serious air pollution problems in China (Lei et al., 2011; Chan et al., 2008). The poor air quality mainly related to the aerosol particles suspended in the near surface air, which could downgrade air quality and visibility, and damage human health (Pope et al., 2002; Peng et al., 2018). As the aerosols strongly absorb and scatter solar radiation over the ultraviolet, visible light, and infrared spectrum, they exert a significant influence on global climate and weather processes (Rosenfeld et al., 2007; Wang et al., 2012).

Aerosol Optical Depth (AOD), a measure of the columnar extinction of solar radiation and long wave radiation by aerosols, is an important optical parameter in estimation of aerosol concentration, evaluation of the level of atmospheric pollution, and assessment of the climate effect of aerosols (He et al., 2014; Lohmann et al., 2006; Hu et al., 2012; Peng et al., 2015; Dai et al., 2014; Dai et al., 2015). To evaluate the effects of aerosols on climate it is necessary to estimate their spatial and temporal distributions.

Recent satellite-based remote sensing of AOD has greatly improved our understanding of aerosols properties (Adhikary et al., 2008). Because of its spatial and temporal coverage, satellite-based aerosol optical depth is the most practical measurement of aerosol amount for global assessments (Anderson et al., 2005; Hu et al., 2013). The satellite remote sensing method is able to generate results over an extensive area in real-time. The gained results can be updated periodically at a relatively short span (He et al., 2014; Mustard et al., 2017). The uneven distribution of conventional ground observation stations makes it more difficult to study the spatial and temporal distribution characteristics of regional aerosols. Such point-specific data are unable to yield a detailed pattern of aerosol spatiotemporal distribution (Dai et al., 2018; Shen and Min, 2015; Xu et al., 2013). Satellite remote sensing method can become a vital addition to supplement ground-based measurement so as to gather accurate aerosol information effectively and quickly (Stengel et al., 2009; Zou et al., 2011). Meteorological satellite can be divided into polar-orbiting and geostationary satellites by different operating orbits. The polar-orbiting satellites products usually have the high spectral resolution and can monitor the global atmospheric environment. However, it can observe the same region only twice a day and so may miss rapidly developing severe storms (Li & Zou, 2017; Qin et al., 2013; Wang et al., 2018). Conversely, geostationary instruments can provide continuous imagery for resolving the evolution of weather phenomena from mesoscale to the convective scale in the observed domain, due to their fixed position relative to Earth's surface and high spatial and temporal resolution (Montmerle et al., 2007; Wang et al., 2018; Xia et al., 2019b).

The Fengyun-4A (FY-4A) meteorological satellite, a next-generation geostationary meteorological satellite, was launched on 11 December 2016. For instance, the Advanced Geosynchronous Radiation Imager (AGRI) aboard FY-4A (AGRI/FY-4A) takes full-disk images at a 15-min interval in 14 spectral bands with the 0.5–4-km resolution. In addition, a full-disc image of aerosol optical depth (AOD) offered by FY-4A covers a large area (80.6°N–80.6°S, 24.1°E–174.7°W) (Yang et al., 2017; Min et al., 2017; Wang et al., 2019).

One method to improve model forecasts of aerosols is data assimilation (DA), which combines observations with numerical model output and can reduce uncertainties of initial aerosol fields. Data assimilation, which an approach first used in generating initial condition for the numerical weather prediction, offers a means to reduce the uncertainties in the estimates of aerosol distributions (Adhikary et al., 2008). Aerosol data assimilation first introduced since 2000 as aerosol and chemical transport models have improved and more aerosol observations have become available. Since then, there has been rapid development in aerosol forecasting systems at many of the world's numerical weather prediction (NWP) centers. Most researchers have assimilated aerosol observations from satellite (Lynch et al., 2016; Sekiyama et al., 2016; Zhang et al., 2011; Liu et al., 2011; Peng et al., 2015; Yumimoto et al., 2016; Fukuda et al., 2013; Saide et al., 2013; Peng et al., 2016; Xia et al., 2019a) to chemical transport models. Both these models showed that the assimilation greatly improved analysis when comparing with independent observations. However, some researchers indicated that AOD derived from polar-orbiting satellites have limited spatial coverage and observation frequencies. While AOD derived from geostationary satellites can overcome these limitations and they also showed positive impact of geostationary data on air quality prediction and implied that future geostationary missions also have potential to greatly contribute to that (Lahoz et al., 2011; Yumimoto, 2013; Zoogman et al., 2014; Wang et al., 2004; Saide et al., 2014).

In this study, we construct an aerosol data assimilation experiment with AOD derived from Fengyun-4 AGRI data and an aerosol data assimilation system (Xia et al., 2019b) based upon GSI. To evaluate the effectiveness in precipitation forecast, this system is applied and tested in a heavy dust storm event occurred over East Asia during 12-14 May 2019. This study represents the first attempt to assimilate FY-4A aerosol observations with a rapid update data assimilation system and then it will be investigated for the analyses and forecasts of the severe dust storm event that occurred over East Asia during 12–14 May 2019. Details are present in the rest of the paper. The next section describes the Fengyun-4 AGRI AOD data. while section 3 details the severe dust storm event and the aerosol DA system setup for FY-4A assimilation such as the quality control, observation error statistics, and background error covariance in GSI systems. Results are presented in sections 4, and a brief discussion regarding meteorological impact on the aerosol forecasts is provided in sections 5.

2. Observation Data

The Fengyun-4 introduces a new generation of Chinese geostationary meteorological satellites, with the first FY-4A launched on 11 December 2016. The FY-4A satellite was equipped with four advanced optical instruments aboard, including an Advanced Geosynchronous Radiation Imager (AGRI), a Geostationary Interferometric Infrared Sounder (GIIRS), a Lightning Mapping Imager (LMI) and Solar X-EUV Imaging Telescope (SXEIT). AGRI has 14 spectral bands from visible to infrared (0.45 -13.8 μm) with high spatial (1 km for visible at nadir, 2 km for near-infrared, and 4 km for remaining infrared) and temporal (full-disk images at the 15-min interval) resolutions. In addition, a full-disc image offered by FY-4A covers a large area (80.6°N–80.6°S, 24.1°E–174.7°W). FY-4 represents an exciting expansion in Chinese geostationary remote sensing capabilities and detailed descriptions of FY-4A along with its products are given by Yang et al. (2017) and Min et al. (2017).

In this study, the level 2 total AOD retrievals over land and sea provided by National Satellite Meteorological Center with a spatial resolution of 4 km from FY-4A sensors on board the AGRI satellites were used. We estimated observation errors to be the retrieval uncertainty attached to the FY-4A AOD data plus a standard deviation calculated as the representative error in the regridding (Zhang et al., 2008; Xia et al., 2019a). The FY-4 AOD retrievals uncertainty ranged from 0.0001 to 0.96, with an average of 0.039. Quality control (QC) and accurate quantification of the systematic bias and random errors of observations arising from the errors in numerical models and instruments are key components in assimilating satellite aerosols. We only assimilated the highest quality AOD retrievals and thinned to the same resolution as the model grid. As suggested by Saide et al. (2014), pixels adjacent to missing values were discarded and only AOD values below 2.5 were used. The observations with innovations exceeding 3 times of the observation error were rejected before minimization to reduce cloud contamination and noise in the data (Xia et al., 2019b; Wang et al., 2018). All QC decisions, observation thinning, and observation error assignments for aerosol observations were made within GSI for all experiments.

To allow comparison of simulation results from FY-4 data, the latest version of the Himawari-8 AOD (Yoshida et al., 2018; Kikuchi et al., 2018; Dai et al, 2019), which are freely available at the website of the Japan Aerospace Exploration Agency (JAXA) Himawari Monitor (http://www.eorc. jaxa.jp/ptree/index.html) were regridded to the resolution of our model and then the Himawari-8 AOD were assimilated in this study. The Aerosol Robotic Network (AERONET; http://aeronet.gsfc.nasa.gov/) provides AOD measured by sun photometers (Holben et al., 1998). Fig 1 shows the locations of Aerosol Robotic Network (AERONET) sites whose data were served as the independent observations in this study.

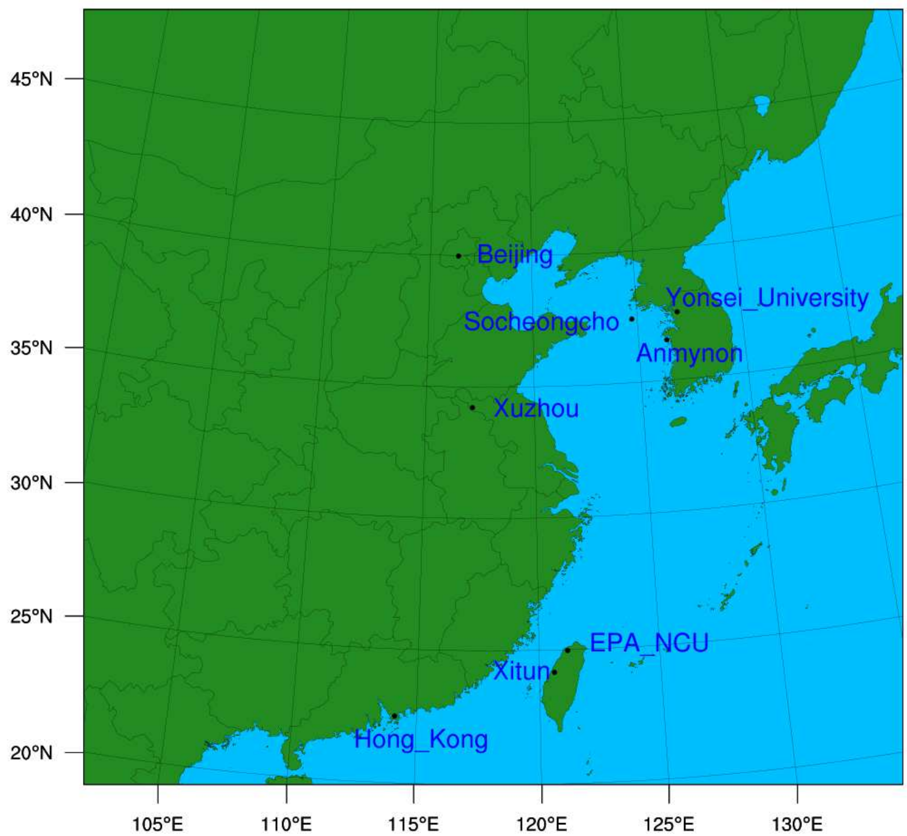

Fig. 1. The experimental domain. Blue labeling indicates the ground-based AOD data

acquired by the AERONET sites used in this study.

3. Experimental Setup

3.1 The Severe Dust Storm Event

The study focused on an extreme dust storm event that occurred over East Asia in the year 2019 over northern China. During 12-14 May 2019, there was a large range of persistent heavy air pollution in large areas of China. The dust storm caused poor visibility, air quality, and flights' cancelation or delays over eastern China. AOD (500 nm) values observed at the Beijing AERONET site varied from less than 1 on 11 May to a maximum of 2 on 12 May, when China was severely affected by the dust storm.

3.2 Aerosol DA system

The Gridpoint Statistical Interpolation (GSI) 3DVAR algorithm is explained by Wu et al. (2002), and its expansion for aerosol DA using the GOCART aerosol module is described by Liu et al. (2011). We added a new interface to the FY-4A AOD data in this study as a follow on work of Liu et al. (2011) and Xia et al. (2019b). The variational method is a well-established approach which combines model background information with observations to obtain the ''best'' forecast possible. This approach is widely used in many NWPs centers. The method is based on minimization of a cost function which measures the distance between observations and their model equivalent, subject to a background constraint usually provided by the model itself (Morcrette et al., 2009). Associated with the background and observations are their error characteristics. Given the background, observations, and errors, the analysis vector (x) can be determined by minimizing a scalar cost-function J(x). The cost function J(x) to be minimized with respect to the bias parameters and model state becomes,

$$J(x)=\frac{1}{2}(x-x_b)^T B^{-1}(x-x_b)+\frac{1}{2}[y-H(x)]^T R^{-1}[y-H(x)] \qquad (1)$$

The covariance matrices determine how closely the analysis is weighted toward the background and observations. H is the potentially nonlinear "observation operator" that interpolates model grid point values to observation locations and transforms model-predicted variables to observed quantities. where B and R are the background and observation error covariance matrices of dimensions $m\times m$ and $p\times p$, respectively. x_b denotes the background vector, y is a vector of observations and B and R determine the relative contributions of the background and observation terms to the final analysis.

The 3DVAR algorithm requires background error covariance (BEC) statistics for each analysis variable. GSI uses recursive filters and permits spatially inhomogeneous BECs (Wu et al., 2002). The BEC were computed for each aerosol species via the "National Meteorological Center (NMC) method" (Parrish and Derber, 1992) by taking the differences of 24 and 12 h Weather Research and Forecasting with

Chemistry (WRF/Chem) forecasts of the 14 aerosol species (including hydrophobic and hydrophilic organic carbon [OC] and black carbon [BC]; sulfate; sea-salt in four particle-size bins (effective radii of 0.3, 1.0, 3.25, and 7.5 μm for dry air); and dust particles in five particle-size bins (effective radii of 0.5, 1.4, 2.4, 4.5, and 8.0 μm)) valid at the same time for 62 pairs valid at either 0000 or 1200 UTC from 11 April 2019 to 11 May 2019.

3.3 Experimental design

In this study, we performed three numerical experiments to evaluate the impact of FY-4 AOD DA on aerosol analyses and forecasts over the East Asia. One experiment ("CNT") served as the control and did not employ any DA. The other two experiments all performed 3DVAR DA but assimilated different observations. The FY-4 AOD data were assimilated by one experiment ("FY DA"), while the other assimilated Himawari-8 AOD observations ("Hima DA"). It is necessary to assimilate high-frequency data at short intervals so that the initial field can contain the information of the dust storm system as much as possible (Xia et al.,2019b). So observations taken within 1 hour of each analysis time were assimilated. In our domain, Himawari-8 AOD provided coverage only 11–12 h d (daytime) (Yumimoto et al., 2016). Thus, the DA experiments only cycled during daylight hours and short forecasts at night.

All observations were assumed to be valid at the analysis time for each experiment.

The model used to simulate the transport of aerosols and chemical species was the WRF-Chem (Grell et al., 2005). The data assimilation and forecast system constructed in this study is based on version 3.8.1 of the WRF-Chem model. As in Liu et al. (2011) and Schwartz et al. (2012), Goddard Chemistry Aerosol Radiation and Transport (GOCART) aerosol scheme was chosen as the aerosol option within WRF-Chem. And then forecasts of 3D mass mixing ratios of 14 aerosol species are produced: hydrophobic and hydrophilic OC and BC; sulfate; sea-salt in four particle-size bins (effective radii of 0.3, 1.0, 3.25, and 7.5 μm for dry air); and dust particles in five particle-size bins (effective radii of 0.5, 1.4, 2.4, 4.5, and 8.0 μm). The experiments were all run over the same domain, which covers main area of east China (Figure 1) and the three experiments were implemented with the same model configuration: 200 × 150 horizontal mesh grid using 20-km spacing and 40 vertical levels up to 50 hPa. The NCAR's MOZART-4 model (Pang, 2012), the Rapid Radiative Transfer Model longwave radiation scheme (Mlawer et al., 1997), the Dudhia shortwave radiation scheme (Dudhia, 1989), Noah land surface model, the Yonsei University (YSU) planetary boundary layer scheme (Hong et al., 2006; Hu et al., 2010) are used for all deterministic forecasts.

The three experiments all initialized a new WRF-Chem forecast every 1 h between 0100 UTC 12 May and 1100 UTC 14 May. The initial aerosol fields were produced by a 5-day forecast, which was needed to overcome the unrealistic of the WRF/Chem forecasting, similar to Pagowski et al. (2010) and Schwartz at al. (2012). Then the newly developed 3DVAR aerosol DA system uses 14 individual aerosol species of the WRF/Chem built-in GOCART module as control variables, including hydrophobic and hydrophilic organic carbon [OC] and black carbon [BC]; sulfate; sea-salt in four particle-size bins (effective radii of 0.3, 1.0, 3.25, and 7.5 μm for dry air); and dust particles in five particle-size bins (effective radii of 0.5, 1.4, 2.4, 4.5, and 8.0 μm). The two experiments that assimilated observations performed a new aerosol analysis every 1 h to update the control variables before initializing WRF-Chem forecasts. The first analyses used the 0100 UTC 12 May fields as backgrounds, while subsequent analyses used the previous cycle's 1h aerosol forecasts as backgrounds. The experiment without DA initialized its first forecast from the 0100 UTC 12 May fields, while initial aerosol fields for future forecasts were simply taken from the previous cycle's 1h forecast. No meteorological DA was performed. Every initialization, all experiments' meteorological fields were updated by interpolating FNL analyses onto the computational domain.

The analyses and forecasts from the three experiments were compared to AOD observations from FY-4, Himawari-8 and AERONET. The results of these comparisons are now described.

4. Results

4.1. Comparison to Fengyun-4 AOD and Himawari-8 AOD

A variety of metrics were used to verified the WRF-Chem forecast. Many statistics assessing forecast accuracy can be defined based on the correspondence between the model and observations (Schwartz at al., 2012). The mean Bias is simply the difference of the mean and observed values and can be considered a measure of systematic model error. The root mean square error (RMSE) could quantify how individual forecast-observation pairs agree and can be interpreted as a measure of non-systematic model error. To evaluate the experiments' ability to discriminate between events, we calculate the average RMSE and Bias between those model fields and the observations. In order to evaluate the overall performance of the DA system, time series of the hourly pollutant concentrations from the CNT forecast, the DA analysis, and the DA forecast of the three experiments were compared with the independent observations in the domain (Fig. 2). In Fig 2, the X-axis presents analysis time, Y-axis presents values of AOD values, Bias and RMSEs. Furthermore, Table 1-3 summarized the statistical analysis of the simulated and observed AOD in the experiments.

In the CNT experiment, it did not perform very well, although it was able to capture the synoptic variability when there was a severe dust event. In order to see the evolution process of aerosol more directly, Time series of the absolute AOD values, Bias and RMSE of the simulated AOD in the FY DA systems and in the Hima DA systems during the period of 12-14 May 2019 were included in Fig. 2. Based on the model performance evaluation statistical metrics, both two assimilation experiments are superior to the CNT experiment, indicating that all of the analyses can better represent the temporal evolution characteristics of aerosols than the CNT experiment. It can be seen from the Fig. 2a and Fig. 2b that after assimilation the AOD value has been significantly improved in both FY DA and Hima DA experiments. These statistics indicate that the DA system was able to adjust the analysis and forecast fields. As shown in the Table 1 and Fig. 2c-2f, there were larger systematic biases and RMSEs for the CNT experiment. The biases were lower than the corresponding observed concentrations, suggesting a significant systematic underestimation of the WRF-Chem simulation. It can be seen that the Bias and RMSE generally reduced with forecast range, indicating that the DA system was well calibrated. After the assimilation of AOD observations, the magnitudes of the bias and the RMSEs decreased. The Biases were near -0.46 in the CNT and near -0.37 after DA; the RMSE were near 0.45 in the CNT and near 0.36 after DA. Thus the Bias and

RMSE reduced about 20% compared to the CNT experiment, indicating that the analysis fields were very close to the observations. Interestingly, in the Hima DA experiment, the Bias and RMSE values were reduced a little more than in the FY DA systems at sometime. These statistics indicate that the DA system was able to adjust the analysis and forecast fields.

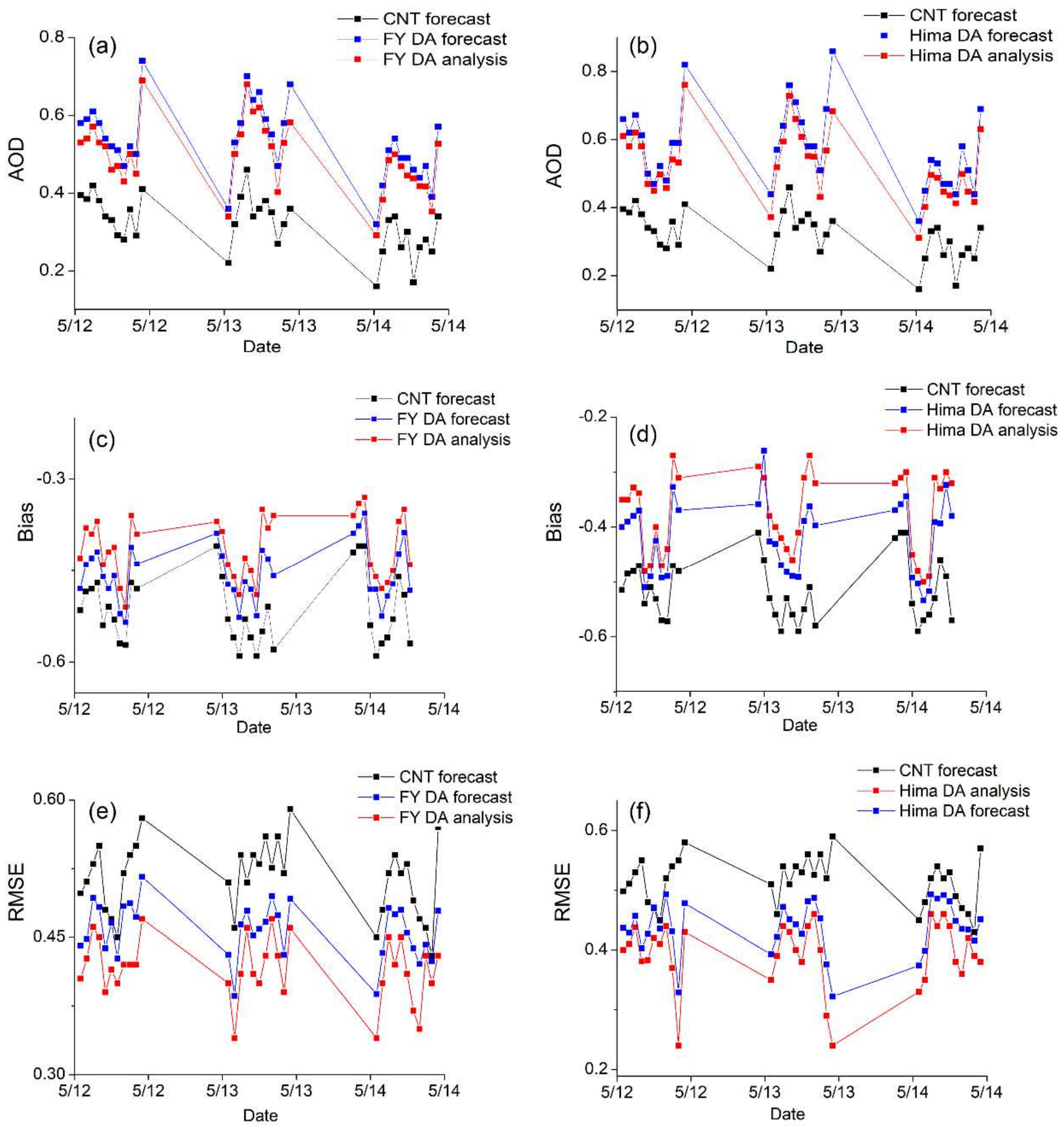

Fig. 2. Time series of the absolute AOD values (a, b), Bias (c, d) and RMSE (e, f) of the simulated AOD. The DA systems involved FY DA AOD data (a, c, e) and Hima DA AOD data (b, d, f) during the period of 12-14 May 2019.

Table 1

Statistical analysis of the simulated and observed AOD in the experiments on 12 May 2019.

Date	FYDA				HimaDA				CNT	
	B_b	B_a	R_b	R_a	B_b	B_a	R_b	R_a	B	R
051201	-0.482	-0.431	0.441	0.405	-0.402	-0.355	0.437	0.407	-0.515	0.498
051202	-0.443	-0.387	0.448	0.427	-0.396	-0.352	0.429	0.413	-0.485	0.511
051203	-0.485	-0.392	0.493	0.461	-0.389	-0.328	0.457	0.438	-0.487	0.534
051204	-0.423	-0.376	0.483	0.452	-0.374	-0.337	0.403	0.381	-0.473	0.551
051205	-0.466	-0.447	0.438	0.391	-0.512	-0.486	0.427	0.383	-0.546	0.488
051206	-0.481	-0.428	0.466	0.415	-0.492	-0.471	0.471	0.426	-0.512	0.472
051207	-0.458	-0.412	0.427	0.409	-0.425	-0.404	0.436	0.415	-0.534	0.453
051208	-0.512	-0.483	0.484	0.428	-0.492	-0.473	0.493	0.442	-0.570	0.526
051209	-0.535	-0.516	0.487	0.426	-0.489	-0.443	0.431	0.375	-0.572	0.540
051210	-0.412	-0.368	0.472	0.423	-0.327	-0.272	0.329	0.249	-0.474	0.557
051211	-0.439	-0.395	0.516	0.477	-0.369	-0.316	0.478	0.433	-0.481	0.589

Table 2

Statistical analysis of the simulated and observed AOD in the experiments on 13 May 2019.

Date	FYDA				HimaDA				CNT	
	B_b	B_a	R_b	R_a	B_b	B_a	R_b	R_a	B	R
051301	-0.389	-0.373	0.431	0.406	-0.358	-0.292	0.356	0.393	-0.422	0.515
051302	-0.268	-0.255	0.386	0.342	-0.261	-0.211	0.422	0.391	-0.417	0.468
051303	-0.473	-0.442	0.464	0.415	-0.426	-0.383	0.472	0.443	-0.416	0.543
051304	-0.482	-0.461	0.479	0.463	-0.431	-0.406	0.451	0.434	-0.543	0.515
051305	-0.527	-0.490	0.411	0.452	-0.469	-0.427	0.443	0.408	-0.597	0.544
051306	-0.469	-0.438	0.459	0.408	-0.482	-0.441	0.427	0.387	-0.575	0.536
051307	-0.481	-0.454	0.467	0.433	-0.465	-0.489	0.481	0.442	-0.564	0.569
051308	-0.524	-0.496	0.495	0.477	-0.466	-0.491	0.487	0.466	-0.533	0.527
051309	-0.417	-0.355	0.474	0.430	-0.312	-0.389	0.453	0.401	-0.460	0.561
051310	-0.412	-0.431	0.431	0.399	-0.277	-0.392	0.376	0.293	-0.494	0.527
051311	-0.458	-0.367	0.388	0.492	-0.184	-0.357	0.322	0.245	-0.571	0.593

Table 3

Statistical analysis of the simulated and observed AOD in the experiments on 14 May 2019.

Date	FYDA				HimaDA				CNT	

	B_b	B_a	R_b	R_a	B_b	B_a	R_b	R_a	B	R
051401	-0.389	-0.365	0.388	0.346	-0.369	-0.325	0.374	0.338	-0.423	0.452
051402	-0.377	-0.346	0.433	0.409	-0.358	-0.317	0.399	0.354	-0.417	0.489
051403	-0.356	-0.332	0.482	0.453	-0.344	-0.306	0.493	0.462	-0.416	0.525
051404	-0.481	-0.443	0.475	0.428	-0.492	-0.452	0.486	0.443	-0.542	0.540
051405	-0.483	-0.469	0.480	0.451	-0.503	-0.489	0.492	0.461	-0.593	0.523
051406	-0.525	-0.486	0.455	0.412	-0.534	-0.502	0.481	0.447	-0.571	0.537
051407	-0.492	-0.472	0.438	0.375	-0.517	-0.491	0.449	0.386	-0.566	0.496
051408	-0.472	-0.451	0.421	0.356	-0.391	-0.314	0.435	0.365	-0.534	0.471
051409	-0.423	-0.378	0.442	0.432	-0.393	-0.332	0.434	0.429	-0.468	0.466
051410	-0.388	-0.353	0.424	0.406	-0.323	-0.306	0.416	0.393	-0.490	0.438
051411	-0.483	-0.440	0.479	0.431	-0.382	-0.328	0.451	0.380	-0.575	0.575

In order to evaluate the improvement of AOD spatial distribution in the initial field by AOD assimilation, we conducted a comparative analysis of the background field and the analysis field, in which the simulation value of AOD was calculated by the extinction coefficient of 550nm wavelength output of the model (Fig. 3). Observations of 1-hour DA windows from FY4, distributions of simulated AOD based on DA the background fields, the analysis fields and the 1-h forecast fields for the FY DA system were displayed in Fig 3a, 3b, 3c and 3d, respectively.

The simulation of the dust storm in the CNT experiment was inadequate (Fig 3b). After the assimilation of the satellite AOD data, the analysis field added the aerosol distribution of the main sources of dust in the dust storm weather - the middle and eastern regions, the north plain and the southern regions of East Asia. The assimilation experiments all reflected the maximum positive increment center of AOD in the region, which was consistent with the distribution of the high value region of

AOD in the satellite observation data. After the assimilation adjustment, the analysis field (Fig 3c) has more abundant observation information, and the aerosol distribution of the analysis field is closer to the satellite observation. The assimilation experiments all reflected the maximum positive increment center of AOD in the region, which was consistent with the distribution of the high value region of AOD in the satellite observation data. After the assimilation adjustment, the analysis field has more abundant observation information, and the aerosol distribution of the analysis field is closer to the satellite observation. As the AOD represents contributions from all aerosol types, so we also plotted the distributions of the dust field (Fig. 4), which gives a direct indication of the dust storm event.

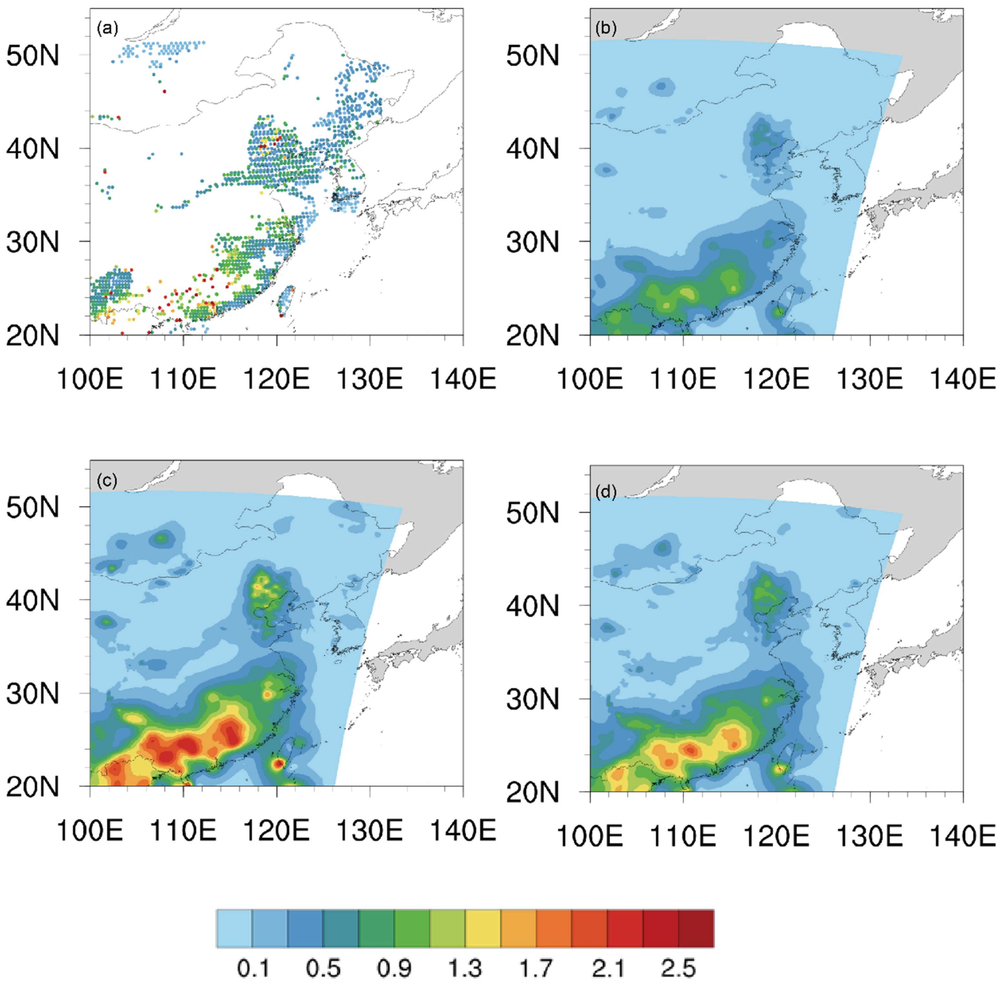

395 Fig.3. Observations of 1-hour DA windows from FY4(a), The result of the control experiment (b), the analysis fields (c) and the 1-h forecast fields (d) for the FY DA system, valid at 0600 UTC 12 May 2019.

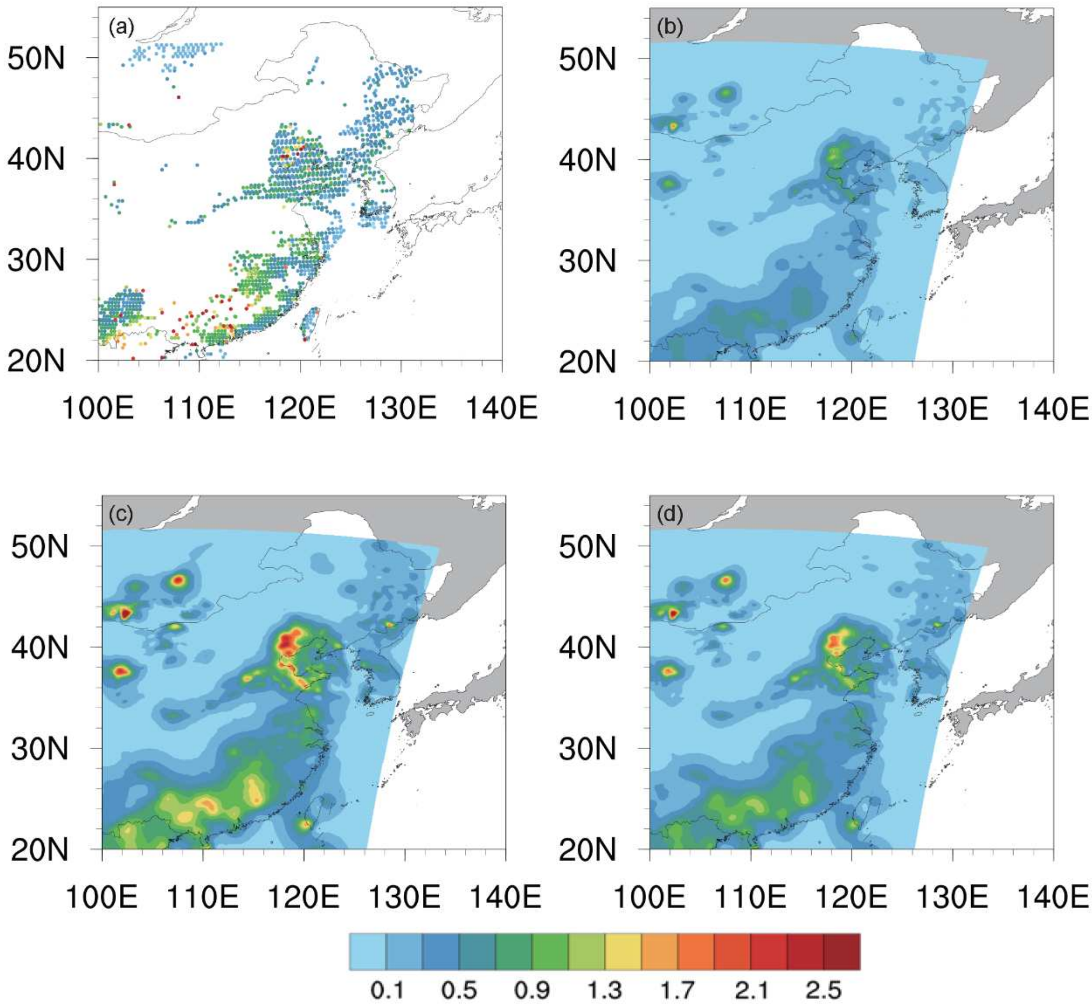

Fig. 4. Observations of 1-hour AOD DA windows from the FY4 (a). The dust fields from CNT experiments (b). Distributions of simulated dust field based on FY DA analysis(c), and the forecast dust fields from FY DA experiments (d), valid at 0600 UTC 12 May 2019. The dust fields here included dust particles in five particle-size bins (effective radii of 0.5, 1.4, 2.4, 4.5, and 8.0 μm).

Similar to Fig. 3, it can be seen that the assimilation of AOD data can predict the distribution of large dust centers in Beijing and Tianjin more accurately, which improving the underestimation of dust values in Beijing and Tianjin in the CNT experiment. At the same time, the addition of observation data also strengthened the distribution of large AOD values in southeast China, Vietnam, northeast China region, making up for the underestimation of CNT and reflecting the real aerosol diffusion and distribution. In general, AOD data assimilation can significantly improve the forecast field, which can improve the intensity and distribution of AOD model, and correct the location of strong center of dust area.

In order to determine the contributions of major aerosol components to the distribution of large value AOD, we showed the spatial distributions of the analysis field of the individual component (i.e., dust, sulfate, organic carbon [OC], black carbon [BC], sea salt, P25 and P10) in the FY-4 assimilation experiments (Fig 5) and in the Himawari-8 assimilation experiments (Fig 6). As shown in Fig. 5 and Fig. 6, the increase of the AOD over the Gobi Desert and Beijing areas for all the two assimilations are all mainly dominated by the dust aerosols, indicating that the underestimation of AOD over the Gobi Desert and Beijing areas in the CNT experiment is mainly caused by the underestimation of dust aerosols. In contrast with the north China, in the south China the large underestimation of AOD of the CNT experiment, which are mainly caused by the underestimation of P25 component, are also removed by the assimilation of the FY-4 AODs and the Himawari□8 AODs. The large P25 component mainly dominated to the AOD over south China in all the two assimilation experiments. All of the analyses correctly increase the AODs to better match the observations.

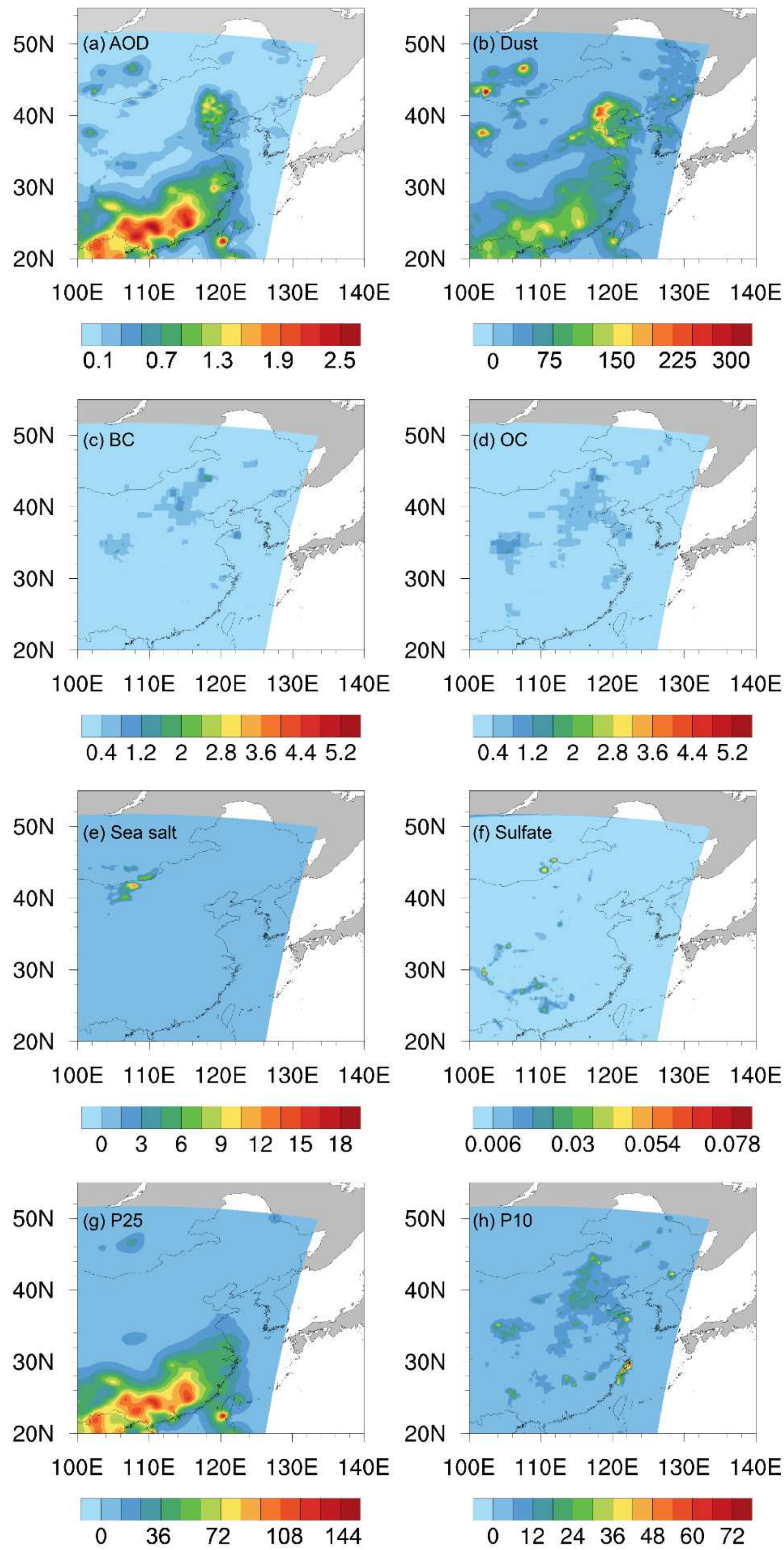

Fig 5. The horizontal distributions of the AOD and the analysis field of individual component (μgkg^{-1}) (i.e., dust (b), sulfate (c), organic carbon [OC] (d), black carbon [BC] (e), sea salt (f), P25 (g) and P10 (h)) in the FY-4 assimilation experiments at 0600 UTC 12 May 2019.

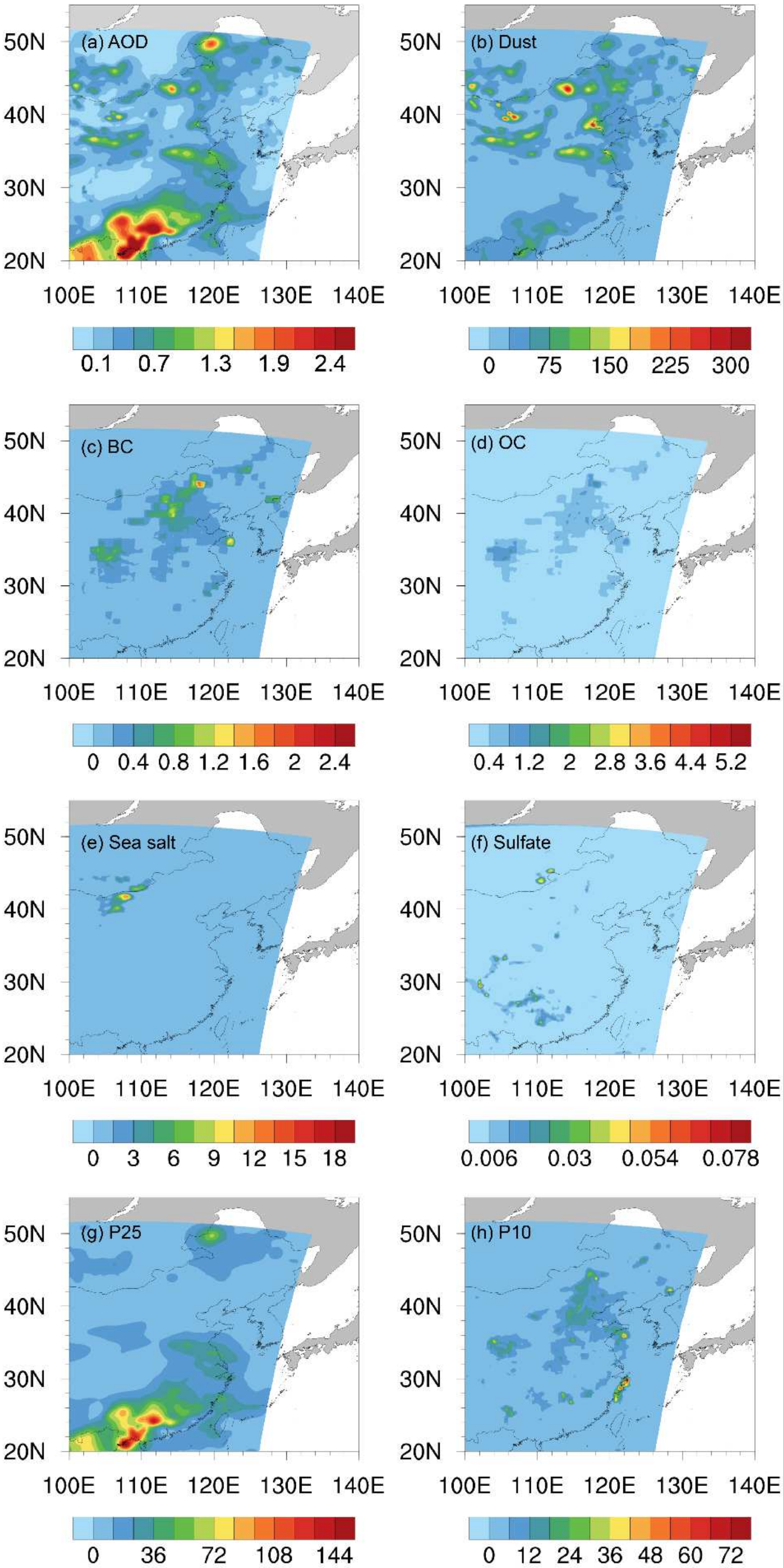

437

438 Fig 6. The horizontal distributions of the AOD (a) and the analysis field of individual
439 component (μgkg^{-1}) (i.e., dust (b), sulfate (c), organic carbon [OC] (d), black carbon [BC] (e),
440 sea salt (f), P25 (g) and P10 (h)) in the Himawari-8 assimilation experiments at 0600 UTC 12
441 May 2019.

4.2. Comparison with AERONET AOD

NASA's Aerosol Robotic Network (AERONET) (Holben et al., 1998; O'Neill et al., 2003) is a well-established ground-based network of models and measurements due to its small wavelength-independent measurement error, with calibration error on the order of 0.015 (Holben et al., 1998; Eck et al., 1999). AERONET data plays an important role in the validation of aerosol satellite remote sensing products and model products.

The ground-based AOD data acquired by AERONET were used to evaluate the assimilation results. Fig 7 shows comparisons of modeled results in the three experiments with AOD from AERONET. The dust storm from 12 May to 14 May 2019 was detected by AERONET at the Anmyon, Beijing, EPA_NCU, Xuzhou, Hong_kong, Socheongcho, Xitun and Yonsei_university sites. At all sites, DA increased AOD values compared to the control and usually agreed better with observations. In some cases, the increase due to DA still was insufficient (e.g., Beijing, EPA_NCU and Xuzhou; Fig 7b, Fig 7c and Fig 7d). As shown in Fig. 7, the hourly assimilation of AOD improves the model predictions. The background model predictions were generally under predicting the observations, which the assimilation corrects for and brings the AOD values after assimilation closer to the AERONET observations. Quite generally speaking, results for AOD in FY-4A and Himawari-8 DA experiments agree better with the observations because of the assimilation. At Anmyon site, we can also see the assimilation improved the underestimation by the CNT experiment. The values in Hima DA were usually larger than those in FY DA and the Hima assimilation overestimate AOD on 13 May. At Beijing site, where more observations are available, there was higher improvements presented. At EPA_NCU and Xuzhou sites, we clearly see a strong positive impact of the assimilation on AOD. The AOD in two DA experiments matched AERONET observations very well in most of the time except when the air pollution reached a high level and the observed AOD value exceeded 1.0. At Hong_kong, Socheongcho, Xitun and Yonsei_university sites, we see little difference on AOD for both FY DA and Hima DA experiments and both agree reasonably well with the independent observations. In general, the result presents good assimilation efficiency to improve the capability of the model to simulate AOD over Eastern Asia.

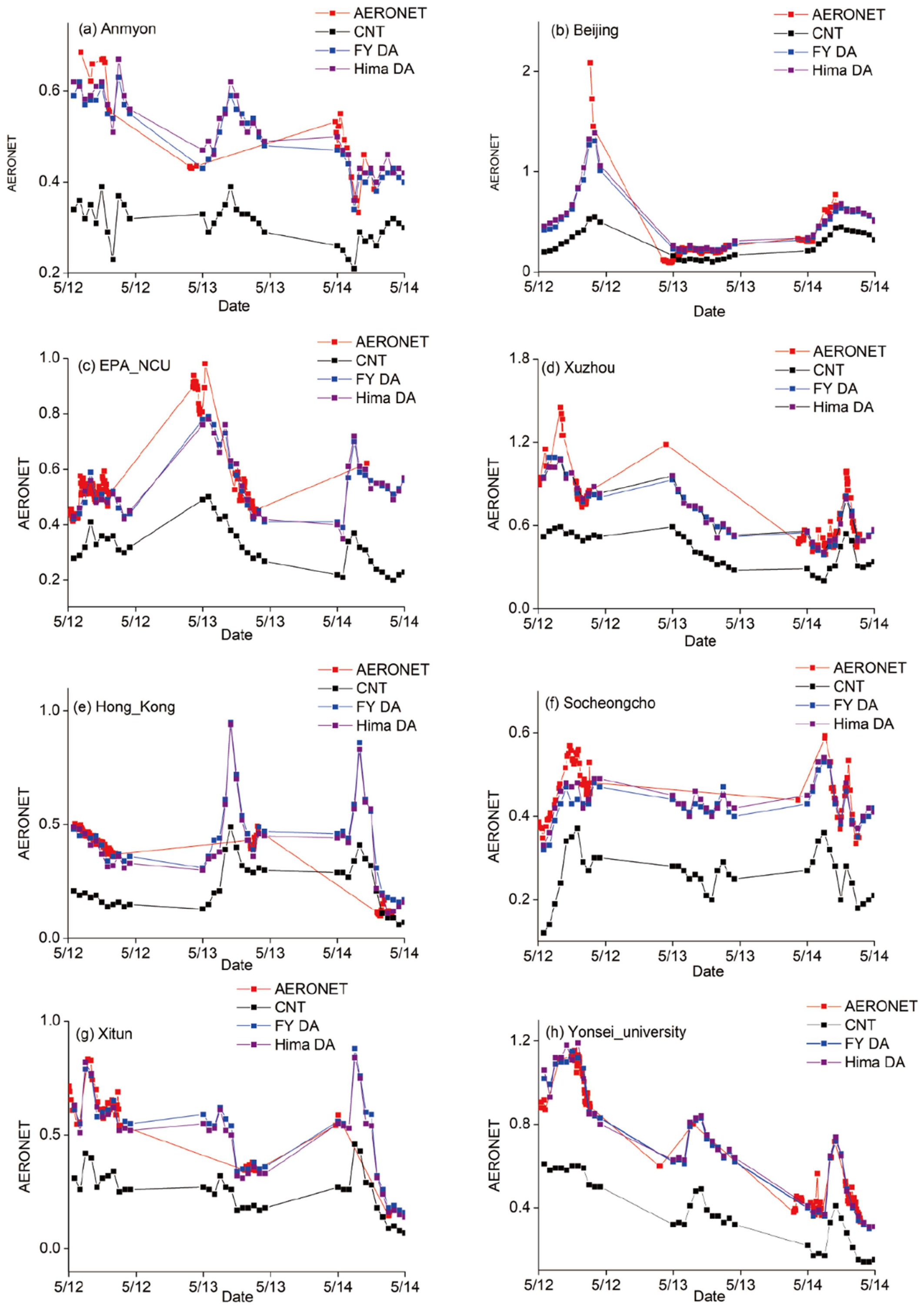

Fig. 7. Comparisons between AERONET retrievals and modeled results in the three experiments from 12 May to 14 May 2019, at the AERONET sites of (a) Anmyon, (b) Beijing, (c) EPA-NCU, and (d) Xuzhou, (e) Hong_Kong, (f) Socheongcho, (g) Xitun, (h) Yonsei_university.

5. Summary and discussion

In this study, the ability of assimilating hourly averaged AOD observations from the FY-4 was added into the aerosol DA framework within the GSI 3DVAR analysis system. Parallel experiments assimilated AOD from FY-4A and Himawari-8 separately and a control experiment that did not employ DA was also performed.

Assimilation of satellite AOD data improved the initial field of the model obviously. AOD assimilation provides the analysis field with more abundant aerosol observation information and more accurate description of the model initial field. AOD data assimilation showed a positive effect on prediction, reasonably improved the intensity and distribution of each variable, and made it more consistent with the observation reality. The statistical results indicated that this assimilation system agreed better with the observations. In addition, aerosol analyses and forecasts with FY-4A AOD DA was substantially improved when compared to independent AOD observations from AERONET sites. The comparison with independent AERONET observations showed that the assimilation can substantially improves modelled AOD. The Bias and RMSE reduced about 20% of the corresponding observed concentrations, indicating that the analysis fields were very close to the observations. The results presented here showed that the FY-4A AOD data assimilation system has a broad development prospect in the application of air quality prediction.

Future developments of the assimilation system will include more advanced DA techniques, high resolution emissions. In the future work, the AOD and PM2.5, PM10 could try to be assimilated together to improve the capability of air pollution forecast.

Acknowledgements

This research was primarily supported by the National Key Research and Development Program of China (Grant Nos. 2017YFC1502100), National Natural Science Foundation of China (41805071,41430427, 41675082), the National Key Research and Development Program of China (2016YFA0602302), the Startup Foundation for Introducing Talent of NUIST (Grant No. 2017r058) and the Priority Academic Program Development of Jiangsu Higher Education Institutions (PAPD).

Reference

Adhikary, B., and Coauthors, 2008, A regional scale chemical transport modeling of Asian aerosols with data assimilation of AOD observations using optimal interpolation technique. Atmos. Environ., 42, 8600–8615, https://doi.org/10.1016/j.atmosenv.2008.08.031.

Anderson, T. L., Charlson, R. J., Bellouin, N., Boucher, O., Chin, M., Christopher, S. A., Haywood, J., Kaufman, Y. J., Kinne, S., Ogren, J. A., Remer, L. A., Takemura, T., Tanre, D., Torres, O., Trepte, C. R., Wielicki, B. A., Winker, D. M., Yu, H., 2005, An 'A-Train' strategy for quantifying direct climate forcing by anthropogenic aerosols. Bulletin of the American Meteorological Society 86 (12), 1795–1809.

Chan, C. K., Yao, X., 2008, Air pollution in mega cities in China. Atmos. Environ. 42, 1–42.

Chandran, V. G. R., Tang, C. F., 2013, The dynamic links between CO2 emissions, economic growth and coal consumption in China and India. Appl. Energy 104, 310–318.

Collins, W. D., Rasch, P. J., Eaton, B. E., Khattatov, B. V., Lamarque, J. F., Zender, C. S., 2001, Simulating aerosols using a chemical transport model with assimilation of satellite aerosol retrievals: methodology for INDOEX. Journal of Geophysical Research Atmospheres 106 (D7), 7313–7336.

Dai, T., Schutgens, N. A. J., Goto, D., Shi, G., Nakajima, T., 2014, Improvement of aerosol optical properties modeling over eastern Asia with MODIS AOD assimilation in a global non-hydrostatic icosahedral aerosol transport model. Environmental Pollution, 195, 319–329.

Dai, T., Cheng, Y., Zhang, P., Shi, G., Sekiguchi, M., Suzuki, K., Goto, D., Nakajima, T., 2018, Impacts of meteorological nudging on the global dust cycle simulated by NICAM coupled with an aerosol model. Atmospheric Environment, 190, 99–115. https://doi.org/10.1016/j.atmosenv.2018.07.016

Dai, T., Shi, G., Nakajima, T. 2015, Analysis and evaluation of the global aerosol optical properties simulated by an online aerosol coupled non-hydrostatic icosahedral atmospheric model. Advances in Atmospheric Sciences, 32, 743–758. https://doi.org/10.1007/s00376-014-4098-z.

Dai, T., Cheng, Y., Suzuki, K., Goto, D., Kikuchi, M., Schutgens, N. A. J., Yoshida, M., Zhang, P., Husi L., Shi, G., Nakajima, T., 2019, Hourly aerosol assimilation of Himawari-8 AOT using the four-dimensional local ensemble transform Kalman filter. Journal of Advances in Modeling Earth Systems,11. https://doi.org/10.1029/2018MS001475

Dudhia, J., 1989, Numerical study of convection observed during the Winter

Monsoon Experiment using a mesoscale two-dimensional model. Journal of the Atmospheric Sciences, 46(20), 3077–3107.

Eck, T. F., Holben, B. N., Reid, J. S., Dubovik, O., Smirnov, A., O'Neill, N. T., Slutsker, I., and Kinne S., 1999, Wavelength dependence of the optical depth of biomass burning, urban, and desert dust aerosols, J. Geophys. Res., 104, 31,333–31,349.

Fukuda, S., Nakajima, T., Takenaka, H., Higurashi, A., Kikuchi, N., Nakajima, T. Y., and Ishida H., 2013, New approaches to removing cloud shadows and evaluating the 380 nm surface reflectance for improved aerosol optical thickness retrievals from the GOSAT/TANSO-Cloud and Aerosol Imager, J. Geophys. Res. Atmos., 118, 13,520–13,531, doi:10.1002/2013JD020090.

He, J., Zha, Y., Zhang, J., Gao, J., 2014, Aerosol Indices Derived from MODIS Data for Indicating Aerosol-Induced Air Pollution. Remote Sensing, 6(2), 1587–1604. doi:10.3390/rs6021587.

Hong, S. Y., Lim, J. O. J., 2006, The WRF single-moment 6-class microphysics scheme (WSM6). Journal of the Korean Meteorological Society,42(2), 129–151.

Holben, B. N., Eck, T. F., Slutsker, I., Tanré, D., Buis, J. P., Setzer, A., Vermote, E., Reagan, J. A., Kaufman, Y. J., Nakajima, T., Lavenu, F., Jankowiak, I, Smirnov, A., 1998, AERONET-A federated instrument network and data archive for aerosol characterization, Remote Sens, Remote Sens. Environ., 66, 1–16, doi:10.1016/S0034-4257(98)00031-5.

Hu, X. M., Doughty, D. C., Sanchez, K. J., Joseph, E., Fuentes, J. D., 2012, Ozone variability in the atmospheric boundary layer in Maryland and its implications for vertical transport model. Atmospheric Environment, 46, 354–364. doi:10.1016/j.atmosenv.2011.09.054

Hu, X. M., Klein, P. M., Xue, M., Zhang, F., Doughty, D. C., Forkel, R., Joseph, E., Fuentes, J. D., 2013, Impact of the vertical mixing induced by low-level jets on boundary layer ozone concentration. Atmospheric Environment, 70, 123–130. doi:10.1016/j.atmosenv.2012.12.046

Hu, X. M., Nielsen-Gammon, J. W., Zhang, F., 2010, Evaluation of three planetary boundary layer schemes in the WRF model. Journal of Applied Meteorology and Climatology 49, 1831e1844.

Kikuchi, M., Murakami, H., Suzuki, K., Nagao, T. M., Higurashi, A., 2018, Improved hourly estimates of aerosol optical thickness using spatiotemporal variability derived from Himawari‐8 geostationary satellite. IEEE Transactions on Geoscience and Remote Sensing, 56(6), 3442−3455. https://doi.org/10.1109/TGRS.2018.2800060.

Lahoz, W. A., Peuch, V.-H., Orphal, J., Attié, J.-L., Chance, K., Liu, X., Edwards, D., Elbern, H., Flaud, J. M., Claeyman, M., Amraoui, L. E., Monitoring air quality from space: The case for the geostationary platform, Bull. Am. Meteorol. Soc., 93(2), 221–233, doi:10.1175/BAMS-D-11-00045.1.

Lei, Y., Zhang, Q., He, K. B., Streets, D. G., 2011, Primary anthropogenic aerosol emission trends for China, 1990–2005. Atmos. Chem. Phys. 11, 931–954.

Li, X., Zou, X., 2017, Bias characterization of CrIS radiances at 399 selected channels with respect to NWP model simulations. Atmospheric Research, 196, 164–181. https://doi.org/10.1016/j.atmosres.2017.06.007

Liu, Z. Q., Liu, H., Lin, C., Schwartz, C. S., Lee, Y. H., Wang, T., 2011, Three-dimensional variational assimilation of MODIS aerosol optical depth: implementation and application to a dust storm over East Asia. J. Geophys. Res. 116, D23206. https://doi.org/10.1029/2011JD016159.

Lohmann, U., 2006, Aerosol effects on clouds and climate. Space Sci. Rev. 125 (1–4), 129–137. Lynch, P., Reid.

Lynch, P., Reid, J. S., Westphal, D. L., Zhang, J., Hogan, T. F., Hyer, E. J., Curtis, C. A., Hegg, D. A., Shi, Y., Campbell, J. R., Rubin, J. I., Sessions, W. K., Turk, F. J., Walker, A. L., An 11-year global gridded aerosol optical thickness reanalysis (v1.0) for atmospheric and climate sciences, Geosci. Model Dev., 9, 1489–1522, doi:10.5194/gmd-9-1489-2016.

Min, M., Wu, C. Q., Li, C., Liu, X., Xu, N., Wu, X., Chen, L., Wang, F., Sun, F., Qin, D., Wang, X., Li, B., Zheng, Z., Cao, G., Dong, L., 2017, Developing the science product algorithm testbed for Chinese next-generation geostationary meteorological satellites: Fengyun-4 series. J. Meteor. Res., 31, 708–719, doi: 10.1007/s13351-017-6161-z.

Mlawer, E. J., Taubman, S. J., Brown, P. D., Iacono, M. J., Clough, S. A., 1997, Radiative transfer for inhomogeneous atmospheres: RRTM, a validated correlated–k model for the longwave. Journal of Geophysical Research, 102(D14), 16,663–16,682. https://doi.org/10.1029/97JD00237

Montmerle, T., Rabier, F., Fischer, C., 2007, Relative impact of polar-orbiting and geostationary satellite radiance in the Aladin/France numerical weather prediction system. Quarterly Journal of the Royal Meteorological Society, 133(624), 655–671. https://doi.org/10.1002/qj.3.

Mustard, J. F., 2017, From planets to crops and back: remote sensing makes sense. J. Geophys. Res. Planets 122 (1), 794–797.O'Neill, N. T., Eck, T. F., Smirnov, A., Holben, B. N., and Thulasiraman, S., 2003, Spectral discrimination of coarse and fine mode optical depth, J. Geophys. Res., 108(D17), 4559, doi:10.1029/2002JD002975.

Pagowski, M., Grell, G. A., McKeen, S. A., Peckham, S. E., and Devenyi. D., 2010, Three-dimensional variational data assimilation of ozone and fine particulate matter observations: Some results using the Weather Research and Forecasting – Chemistry model and Grid-point Statistical Interpolation, Q. J. R. Meteorol. Soc., 136, 2013–2024, doi:10.1002/qj.700

Pang, Y., 2012, Distribution and evolution of atmospheric pollutants over Beijing-Tianjin-Hebei region. M.S. thesis, Nanjing University of Information Science & Technology.

Parrish, D. F., and Derber, J. C., 1992, The national meteorological center's spectral statistical-interpolation analysis system. Mon. Wea. Rev., 120, 1747--1763, https://doi.org/10.1175/1520-0493(1992)120<1747:TNMCSS>2.0.CO;2

Peng, Z., Zhang, M., Kou, X., Tian, X., and Ma, X., 2015, A regional carbon data assimilation system and its preliminary evaluation in East Asia, Atmos. Chem.

Phys., 15, 1087–1104, https://doi.org/10.5194/acp-15-1087-2015

Peng, Z., Lei, L., Liu, Z., Sun, J., Ding, A., Ban, J., Chen, D., Kou, X., and Chu, K., 2018, The impact of multi-species surface chemical observation assimilation on air quality forecasts in China, Atmos. Chem. Phys., 18, 17387-17404, https://doi.org/10.5194/acp-18-17387-2018.

Peng, Z., Liu, Z., Chen, D., Ban, J., 2016, Improving PM2.5 forecast over China by the joint adjustment of initial conditions and source emissions with an ensemble Kalman, Atmospheric Chemistry and Physics, 17:1-35.

Pope, C. A., Burnett, R. T., Thun, M. J., Calle, E. E., Krewski, D., Ito, K., and Thurston., G. D., 2002, Lung cancer, cardiopulmonary mortality, and long-term exposure to fine particulate air pollution, J. Am. Med. Assoc., 287(9), 1132–1141, doi:10.1001/jama.287.9.1132.

Qin, Z., Zou, X., Weng, F., 2013, Evaluating added benefits of assimilating GOES imager radiance data in GSI for coastal QPFs. Monthly Weather Review, 141(1), 75–92. https://doi.org/10.1175/MWR-D-12-00079.1

Rosenfeld, D., Dai, J., Yu, X., Yao, Z. Y., Xu, X. H., Yang, X., Du, C. L., 2007, Inverse relations between amounts of air pollution and orographic precipitation. Science, 315, 1396–1398.

Saide, P. E., Carmichael, G. R., Liu, Z., Schwartz, C. S., Lin, H.-C., da Silva, A. M., and Hyer E., 2013, Aerosol optical depth assimilation for a size resolved sectional model: Impacts of observationally constrained, multi-wavelength and fine mode retrievals on regional scale forecasts, Atmos. Chem. Phys. Discuss., 13, 12,213–12,261, doi:10.5194/acpd-13-12213-2013.

Saide, P. E., Kim, J., Song, C. H., Choi, M., Cheng, Y., and Carmichael, G. R., 2014, Assimilation of next generation geostationary aerosol optical depth retrievals to improve air quality simulations, Geophys. Res. Lett., 41, 9188–9196, doi:10.1002/2014GL062089.

Schwartz, C. S., Liu, Z., Lin, H.-C., and McKeen S. A., 2012, Simultaneous three-dimensional variational assimilation of surface fine particulate matter and

MODIS aerosol optical depth, J. Geophys. Res., 117, D13202, doi:10.1029/2011JD017383

Schwartz, C. S., Liu, Z., Lin, H.-C., and Cetola J. D., 2014, Assimilating aerosol observations with a “hybrid” variational-ensemble data assimilation system, J. Geophys. Res. Atmos., 119,4043–4069, doi:10.1002/2013JD020937.

Sekiyama, T., Yumimoto, T., Tnanaka, K., Nagao, T. M., Kikuchi, M., and Murakami, H., 2016, Data assimilation of Himawari-8 aerosol observations: Asian dust forecast in June 2015, Sola, 12, 86–90, doi:10.2151/sola.2016-020.

Shen, F., Min, J., 2015, Assimilating AMSU-a radiance data with the WRF hybrid En3DVAR system for track predictions of Typhoon Megi (2010). Advances in Atmospheric Sciences, 32(9), 1231–1243. https://doi.org/10.1007/s00376-014-4239-4.

Skamarock, W. C., Klemp, J. B., Dudhia, J., Gill, D. O., Barker, D. M., Duda, M. G., Huang, X.-Y., Wang, W., and Powers J. G., 2008, A description of the Advanced Research WRF version 3, NCAR Tech Note NCAR/TN-475+STR, 113 pp. NOAA, Boulder, Colo.

Stengel, M., Undén, P., Lindskog, M., Dahlgren, P., Gustafsson, N., Bennartz, R., 2009, Assimilation of SEVIRI infrared radiance with HIRLAM 4D-Var. Quarterly Journal of the Royal Meteorological Society, 135(645), 2100–2109. https://doi.org/10.1002/qj.501

Wang, J., Nair, U., and Christopher, S., 2004, GOES 8 aerosol optical thickness assimilation in a mesoscale model: Online integration of aerosol radiative effects, J. Geophys. Res., 109, D23203, doi:10.1029/2004JD004827.

Wang, T., Luo, J., Liang, J., Wang, B., Tian, W., Chen, X., 2019, Comparisons of AGRI/FY-4A Cloud Fraction and Cloud Top Pressure with MODIS/Terra Measurements over East Asia. Journal of Meteorological Research, 33(4), 705–719. doi:10.1007/s13351-019-8160-8

Wang, K. C., Dickinson, R. E., Liang, S. L., 2009, Clear sky visibility has decreased over land globally from 1973 to 2007. Science, 323, 1468–1470.

Wang, Y., Liu, Z., Yang, S., Min, J., Chen, L., Chen, Y., Zhang, T., 2018, Added Value of Assimilating Himawari-8 AHI Water Vapor Radiances on Analyses and Forecasts for “7.19” Severe Storm Over North China. J. Geophys. Res. Atmos. 123 (7), 3374–3394.

Wu, W.-S., Parrish, D. F., and Purser, R. J., 2002, Three-dimensional variational analysis with spatially inhomogeneous covariances, Mon. Weather Rev., 130, 2905–2916.

Xia, X. L., Min, J., Shen, F., Wang, Y., Yang, C., 2019a, Aerosol data assimilation using data from Fengyun-3A and MODIS: Application to a dust storm over East Asia in 2011. Adv. Atmos. Sci., 36(1), 1–14, https://doi.org/10.1007/s00376-018-8075-9.

Xia, X., Min, J., Wang, Y., Shen, F., Yang, C., Sun, Z., 2019b, Assimilating Himawari-8 AHI aerosol observations with a rapid-update data assimilation system. Atmospheric Environment, 116866. doi:10.1016/j.atmosenv.2019.116866.

Xu, D., Liu, Z., Huang, X., Min, J., Wang, H., 2013, Impact of assimilation IASI radiances on forecasts of two tropical cyclones. Meteorology and Atmospheric Physics, 122(1–2), 1–18. https://doi.org/10.1007/s00703-013-0276-2.

Yang, J., Zhang, Z., Wei, C., Lu, F., Guo, Q., 2017, Introducing the new generation of Chinese geostationary weather satellites, Fengyun-4. Bull. Amer. Meteor. Soc., 98, 1637–1658, doi: 10.1175/BAMS-D-16-0065.1.

Yoshida, M., Kikuchi, M., Nagao, T. M., Murakami, H., Nomaki, T., Higurashi, A., 2018, Common retrieval of aerosol properties for imaging satellite sensors. Journal of the Meteorological Society of Japan, 96B(0), 193 – 209. https://doi.org/10.2151/ jmsj.2018-039.

Yumimoto, K., Kikuchi, N. M., Sekiyama, T. T., Murakami, H., Tanaka, T. Y., Ogi, A., Irie, H., Khatri, P., Okumura, H., Arai, K., Morino, I., Uchino, O., Maki, T., 2016, Aerosol data assimilation using data from Himawari-8, a next-generation geostationary meteorological satellite. Geophys. Res. Lett. 43. https://doi.org/10.1002/2016GL069298

Yumimoto, K., 2013, Impacts of geostationary satellite measurements on CO forecasting: an observing system simulation experiment with GEOS-Chem/LETKF data assimilation system. Atmos. Environ. 74, 123–133. https://doi.org/10.1016/j. atmosenv. 2013.03.032.

Zhang, J. L., Reid, J. S., Westphal, D. L., Baker, N. L., and Hyer, E. J., 2008, A system for operational aerosol optical depth data assimilation over global oceans. J. Geophys. Res., 113, D10208, https://doi.org/10.1029/2007JD009065.

Zhang, P., Guo, Q., Chen, B. Y., Feng, X., 2015, The Chinese Next-Generation Geostationary Meteorological Satellite FY-4 Compared with the Japanese Himawari-8/9 Satellites. Advances in Meteorological Science and Technology., 6(1)-2016. doi: 10.3969/j.issn.2095-1973.2016.01.010.

Zhang, M., Zhang, F., Huang, X.-Y., and Zhang X., 2011, Inter-comparison of an ensemble Kalman filter with three- and four-dimensional variational data assimilation methods in a limited-area model over the month of June 2003, Mon. Weather Rev., 139, 566–572.

Zoogman, P., Jacob, D. J., Chance, K., Liu, X., Lin, M., Fiore, A., and Travis, K., 2014, Monitoring high-ozone events in the US Intermountain West using TEMPO geostationary satellite observations, Atmos. Chem. Phys., 14(12), 6261–6271, doi:10.5194/acp-14-6261-2014.

Zou, X., Qin, Z., Weng, F., 2011, Improved coastal precipitation forecasts with direct assimilation of GOES-11/12 imager radiance. Monthly Weather Review, 139(12), 3711–3729. https://doi.org/10.1175/MWR-D-10-05040.1

Highlights

1) It is the first attempt to assimilate FY-4A AOD with a rapid-update DA system.
2) It was investigated for the dust storm occurred over East Asia on 12-14 May 2019.
3) General positive impacts were achieved from assimilating high-frequency data.

Declaration of interests

☑The authors declare that they have no known competing financial interests or personal relationships that could have appeared to influence the work reported in this paper.

☐The authors declare the following financial interests/personal relationships which may be considered as potential competing interests:

Sincerely,

Xiaoli Xia, Jinzhong Min, Feifei Shen, Yuanbing Wang, Dongmei Xu, Chun Yang, Peng Zhang

Nanjing University of Information Science & Technology

No.219 Ningliu Road, Nanjing, Jiangsu Province, 210044, P.R. China

xiaxl@nuist.edu.cn